Chem. Mater. **2004,** *16,* 1775−1785

Protein−Ligand Mediated Aggregation of Nanoparticles: A Study of Synthesis and Assembly Mechanism

Philip J. Costanzo,[†] Timothy E. Patten,[*,†] and Thomas A. P. Seery[‡]

Department of Chemistry, University of California at Davis, One Shields Avenue,
Davis, California 95616-5295, and Institute of Materials Science, University of Connecticut,
97 North Eagleville Road, U-136, Storrs, Connecticut 06269-3136

Received February 4, 2004

Two difunctional, asymmetric PEG linkers were synthesized and utilized to prepare water-soluble, biotinylated CdS@SiO$_2$ particles with various surface contents of the biotin groups. Aqueous dispersions of these particles were prepared, and upon addition of avidin, aggregation was observed using DLS, TEM, and SEM analysis. The resulting aggregates were dense but also had fractal shapes. It was shown that single-angle DLS measurements at 90° were sufficiently accurate for quickly measuring the size of the aggregates as it evolved with time. Initial aggregation rates were measured as a function of surface biotin content of the nanoparticles and initial avidin concentration. The initial rates displayed bell-shaped curve responses to variations in the avidin-to-particle ratio and biotin-to-avidin ratio, the shapes of which were attributed to the stoichiometric balance/imbalance of the avidin-to-biotin ratio in the system and to intraparticle and interparticle bridges that could sterically block avidin from reaching some biotin sites. The growth mechanism was postulated to be a step-growth process.

Introduction

Investigations into the assembly/aggregation of nanoparticles are motivated by an interest in building materials and devices incorporating nanoparticles, with their unique optical and magnetic properties, as components. Such aggregation processes are used to build nanostructures, to sense small concentrations of other biological molecules, and to tag or image cells/tissues in vitro and in vivo. There are several different methods to create nanostructures that utilize self-assembling processes, such as hydrophobic/hydrophilic interactions,[1−3] the interaction of complimentary functional groups,[4−7] the interaction of complimentary biological components,[8−12] the formation of coordination complexes,[4,13,14] or the formation of covalent bonds.[11,15−21] The concept of “programmed assembly” involves using known specific interactions between biological molecules to direct the aggregation of building blocks into a structure. When one of the key components is an analyte, then the formation of a structure is a mechanism by which biological or chemical species can be sensed. Such phenomena have been used in latex immunoglutination and recently quantum dot immunoglutination, and there have been many other examples of programmed assembly through the formation of duplex DNA, protein−ligand interactions, and antibody−hapten interactions.[22−30] Nanoparticles have also

---

* Corresponding author. E-mail: patten@indigo.ucdavis.edu.
† University of California at Davis.
‡ University of Connecticut.

(1) Bowden, N. B.; Weck, M.; Choi, I. S.; Whitesides, G. M. *Acc. Chem. Res.* **2001**, *34*, 231.

(2) Oliver, S. R. J.; Clark, T. D.; Bowden, N.; Whitesides, G. M. *J. Am. Chem. Soc.* **2001**, *123*, 8119.

(3) Mao, C.; Thalladi, V.; Wolfe, D. B.; Whitesides, S.; Whitesides, G. M. *J. Am. Chem. Soc.* **2002**, *124*, 14508.

(4) Norsten, T. B.; Frankamp, B. L.; Rotello, V. M. *Nano Lett.* **2002**, *2*, 1345−1348.

(5) Boal, A. K.; Gray, M.; Ilhan, F.; Clavier, G. M.; Kapitzky, L.; Rotello, V. M. *Tetrahedron* **2002**, *58*, 765−770.

(6) Carroll, J. B.; Krankamp, B. L.; Rotello, V. M. *J. Chem. Soc., Chem. Commun.* **2002**, 1892−1893.

(7) Shenhar, R.; Rotello, V. M. *Acc. Chem. Res.* **2003**, *36*, 549−561.

(8) Li, M.; Wong, K. W.; Mann, S. *Chem. Mater.* **1999**, *11*, 23.

(9) Mann, S.; Shenton, W.; Li, M.; Connolly, S.; Fitzmaurice, D. *Adv. Mater.* **2000**, *12*, 147.

(10) Connolly, S.; Fitzmaurice, D. *Adv. Mater.* **1999**, *11*, 1202.

(11) Um, S. H.; Lee, G. S.; Lee, Y.-J.; Koo, K.-K.; Lee, C.; Yoon, K. B. *Langmuir* **2002**, *18*, 4455.

(12) Lee, G. S.; Lee, Y.-J.; Choi, S. Y.; Park, Y. S.; Yoon, K. B. *J. Am. Chem. Soc.* **2000**, *122*, 12151.

(13) Novak, J. P.; Feldheim, D. L. *J. Am. Chem. Soc.* **2000**, *122*, 3979−3980.

(14) Teranishi, T.; Haga, M.-A.; Shiozawa, Y.; Miyake, M. *J. Am. Chem. Soc.* **2000**, *122*, 4237−4238.

(15) Choi, S. Y., Lee, Y.-J., Park, Y. S., Ha, K., Yoon, K. B. *J. Am. Chem. Soc.* **2000**, *122*, 5201.

(16) Ha, K.; Lee, Y.-J.; Chun, Y. S.; Park, Y. S.; Lee, G. S.; Yoon, K. B. *Adv. Mater.* **2000**, *12*, 1614.

(17) Ha, K.; Lee, Y.-J.; Lee., H. J.; Yoon, K. B. *Adv. Mater.* **2000**, *12*, 1114.

(18) Ha, K.; Lee, Y.-J.; Jung, D.-Y.; Lee, J. H.; Yoon, K. B. *Adv. Mater.* **2001**, *13*, 594.

(19) Kulak, A., Park, Y. S., Lee, Y.-J., Chun, Y. S., Ha, K., Yoon, K. B. *J. Am. Chem. Soc.* **2000**, *122*, 9308.

(20) Lee, G. S., Lee, Y.-J., Ha, K., Yoon, K. B. *Tetrahedron* **2000**, *56*, 6965.

(21) Lee, G. S., Lee, Y.-J., Yoon, K. B. *J. Am. Chem. Soc.* **2001**, *123*, 9769.

(22) Coffer, J. L.; Bigham, S. R.; Li, X.; Pinizzotto, R. F.; Rho, Y. G.; Pirtle, R. M.; Pirtle, I. L. *Appl. Phys. Lett.* **1996**, *69*, 3851−3853.

(23) Niemeyer, C. M.; Burger, W.; Peplies, J. *Angew. Chem. Intl. Ed. Engl.* **1998**, *37*, 2265.

(24) Mirkin, C. A.; Letsing, R. L.; Mucic, R. C.; Storhoff, J. J. *Nature* **1996**, *382*, 607.

(25) Alivisatos, A. P.; Johnsson, K. P.; Peng, X.; Wilson, T. E.; Loweth, C. J.; Bruchez, M. P.; Schultz, P. G. *Nature* **1996**, *382*, 609−611.

(26) Lee, S.-W.; Mao, C.; Flynn, C. E.; Belcher, A. *Science* **2002**, *296*, 892.

10.1021/cm049811i CCC: $27.50

Scheme 1. Synthetic Route Affording Difunctional PEG Linkers[a]

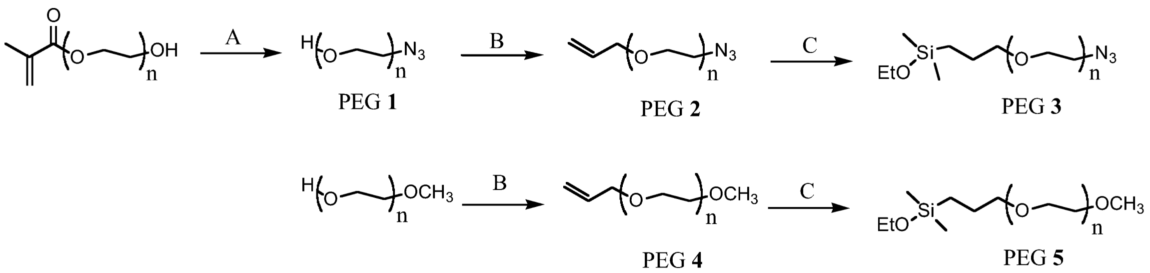

[a] Conditions: (A) (i) CH_3OH, *n*-propylamine, 12 h; (ii) THF, MsCl, Et_3N, 4 h; (iii) H_2O, $NaHCO_3$, NaN_3, 8 h; (iv) K_2CO_3, 12 h. (B) (i) NaH, THF, PEG linker, 1 h; (ii) allyl bromide, 5 h. (C) THF, Karstedt's catalyst, dimethylethoxysilane, 18 h

been assembled onto cell structures in imaging processes.[31,32] With the growth in the number of examples of the biological ligation of nanoparticles, a need had arisen to understand better the processes and mechanisms by which programmed-assembly aggregates form and grow and what types of structures are accessible.

On a molecular interaction basis, programmed assembly is analogous to step-growth polymerization. Two multivalent species with complimentary chemical functionality are allowed to interact and evolve into macromolecular aggregates. If the two species are bifunctional, then cyclic and linear species are formed, or if one or both of the species contain more than two functional groups, then branched or network structures are formed. An example of such an aggregation process was reported by Yoon et al. and involved zeolite crystals as the nanosized building blocks and both covalent bonding[11,15−21] and biochemical interactions[11,12] to provide the cross-linking chemistry. These and other examples provide direction in the types of systems that can be used for programmed assembly.

We report the synthesis of a programmed assembly system and experimental evidence for the mechanism of the aggregation and growth process. This relatively simple system involves spherical CdS@SiO_2 nanoparticles surface modified with biotin end-functionalized poly(ethylene glycol) and avidin as the two components. The CdS@SiO_2−PEG−biotin nanoparticles could be dispersed homogeneously prior to the addition of avidin, which simplified the study of the aggregation process and the determination of optimum conditions for the selective formation of nanoaggregates.

Results and Discussion

Poly(ethylene glycol) (PEG) commonly serves as a linker in biochemical applications, because of its biocompatibility, water solubility, and chain mobility,[33] and it interfaces with biological systems without affecting their function or catalytic activity. PEG linkers have been employed to disperse both CdSe[34] and CdS@SiO_2[35] nanoparticles. The synthesis of asymmetric PEGs with dual reactive end groups has been challenging, though. Typical synthetic procedures either involve statistical functionalization of the chain ends of a symmetric PEG[34,36,37] or start with expensive commercial asymmetric PEG derivatives. Recently, Schwabacher[38] demonstrated a simple route to prepare an α-amino-*ω*-azide PEG linker, whose purification required simple organic extractions, resulting in higher yields and throughput. In this work, a new synthetic route was developed to prepare α-dimethylethoxysilyl-*ω*-functional PEG linkers from a relatively inexpensive, commercially available asymmetric PEG (Scheme 1).

The starting material, α-methacrolyl-*ω*-hydroxy PEG, was treated with *n*-propylamine in order to remove the α,*β*-unsaturated ester functionality. Preliminary attempts at the synthesis bypassed the Michael addition step, but poor yields were obtained in subsequent steps due to polymerization of the methacrylate chain end. The resulting insoluble gels were difficult to manipulate and hindered isolation of the PEG derivatives after saponification of the gels. Consequently, the most convenient reaction conditions and highest yields were obtained by removing the α,*β*-unsaturation via Michael addition while the ester functionality was maintained as a protecting group. The hydroxyl end group at the *ω*-chain end was converted to the mesylate and then treated with NaN_3 to yield the azido end group. The ester group at the α-chain end was removed by saponification with aqueous K_2CO_3 to yield an α-hydroxy-*ω*-azido PEG (PEG-**1**) in good yield and throughput. The hydroxyl end group at the α-chain end of PEG-**1** was converted to the allyl ether by treatment with NaH and allyl bromide in THF. The α-allyloxy-*ω*-azido PEG (PEG-**2**) was then treated with ethoxydimethylsilane and Karstedt's catalyst to form the α-dimethylethoxysilyl-*ω*-azido PEG (PEG-**3**) in an overall yield of 76%, based on starting materials. A second α-dimethylethoxysilyl PEG with an unreactive *ω*-methoxy chain end (PEG-**5**) was prepared in 80% overall yield from a commercially available α-hydroxy-*ω*-methoxy PEG via

---

(27) Seeman, N. C.; Belcher, A. M. *Proc. Natl. Acad. Sci.* **2002**, *99*, 6451.

(28) Lee, S.-W.; Lee, S. K.; Belcher, A. M. *Adv. Mater.* **2003**, *15*, 689.

(29) Mirkin, C. A. *Inorg. Chem.* **2000**, *39*, 2258.

(30) Park, S.-J.; Lazarides, A. A.; Mirkin, C. A.; Letsinger, R. L. *Angew. Chem. Intl. Ed. Engl.* **2001**, *40*, 2909.

(31) Bruchez, M. P., Jr.; Moronne, M.; Gin, P.; Weiss, S.; Alivisatos, A. P.,*Science* **1998**, *281*, 2013−2016.

(32) Chan, W. C. W.; Nie, S. *Science* **1998**, *281*, 2016−2018.

(33) Harris, J. M. *Poly(ethylene glycol) Chemistry: Biotechnical and Biomedical Applications;* Plenum Press: New York, 1992.

(34) Skaff, H.; Emrick, T. *J. Chem. Soc., Chem. Commun.* **2003**, 52.

(35) Parak, W. J.; Gerion, D.; Zanchet, D.; Woerz, A. S.; Pellegrino, T.; Micheel, C.; Williams, S. C.; Seitz, M., Bruehl; R. E., B., Z.; Bustamant, C.; Bertozzi, C. R.; Alivisatos, A. P. *Chem. Mater.* **2002**, *14*, 2113.

(36) Sashiwa, H.; Shigemasa, Y.; Roy, R. *Macromolecules* **2000**, *33*.

(37) Bertozzi, C. R.; Bednarski, M. D. *J. Org. Chem.* **1991**, *56*, 4326.

(38) Schwabacher, A. W.; Lane, J. W.; Schiesher, M. W.; Leigh, K. M.; Johnson, C. W. *J. Org. Chem.* **1998**, *63*, 1727.

Table 1. Nanoparticles Surface Functionalized Using Varying Stoichiometries of PEG-3 and PEG-5

sample	feed ratio[a]	% N for $CdS@SiO_2$-PEG-N_3	N_3 per particle	% N for $CdS@SiO_2$-PEG-NH_2	NH_2 per particle
1	100:0	0.29	2700	0.11	3100
2	66:33	0.24	2300	0.07	2000
3	33:66	0.08	1130	0.04	940
4	10:90	0.01	200	undetectable[b]	200[c]
5	0:100	0	0	0	0

[a] Ratio of PEG-**3** to PEG-**5**. [b] Below the detection limit of elemental analysis. [c] Assumed value based on data from the corresponding azido sample.

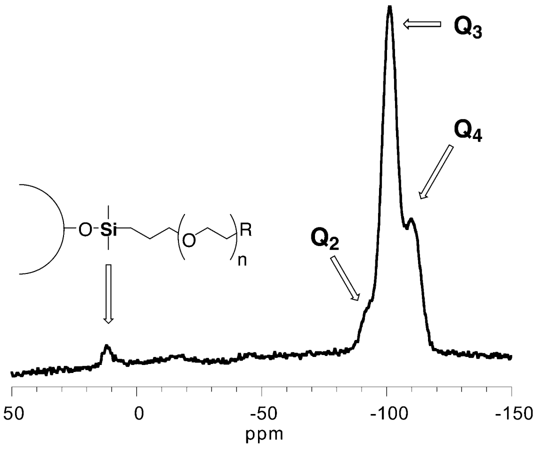

Figure 1. Solid-state ^{29}Si CP-MAS NMR spectrum of modified $CdS@SiO_2$ nanoparticles demonstrating the presence of the PEG chain Si nucleus at 11.9 ppm. (Note: R represents N_3 or OCH_3.)

formation of the allyl ether and then hydrosilation with ethoxydimethylsilane.

Silica-coated CdS nanoparticles were prepared using a previously reported method,[39] and the surfaces of the nanoparticles were derivatized using varying stoichiometries of PEG-**3** and PEG-**5**. These reactions generated a series of surface-functionalized particles in which the relative content of reactive azido groups to inert methoxy groups was varied from 0 to 100% (Table 1).

Solid-state ^{29}Si CP-MAS NMR spectroscopy, IR spectroscopy, and elemental analyses were performed in order to confirm the incorporation of PEG-**3** and PEG-**5** onto the particle surfaces and to provide quantitative information on the reactive functional group content. In the solid-state ^{29}Si CP-MAS spectra (Figure 1), signals were observed at −93.8, −101.2, and −109.9 ppm that were assigned to the Q^2, Q^3, and Q^4 silicon nuclei, respectively, of bulk silica. A signal was observed at 11.9 ppm that was assigned to the surface Si nuclei with three carbon substituents and is consistent with previously assigned ^{29}Si signals.[40] In the IR spectra, an intense signal was observed at 2110 cm^{-1} that confirmed the presence of the azide groups on the particles. Elemental analyses demonstrated the incorporation of nitrogen and were also used to quantify the number of azide functional groups per particle (Table 1).

The nanoparticle surfaces were conjugated with biotin via several steps (Scheme 2). Staudinger reduction of the azide chain ends using PPh_3 in H_3PO_4 and THF yielded the primary amine chain ends, as shown by a two-thirds reduction of nitrogen in the elemental analyses relative to the corresponding azide-containing samples (Table 1) and by the disappearance in the IR spectra of the azide vibration signal at 2110 cm^{-1}. Next, the carboxylic acid group of biotin was activated with *O*-(*N*-succinimidyl)-*N*,*N*,*N*′,*N*′-tetramethyluronium tetrafluoroborate (TSTU), and addition of this solution to a suspension of the amine-terminated nanoparticles yielded an amide linkage between the two components.

Scheme 2. Transformation on the Nanoparticle Surface of the Azido Chain End into a Biotin Chain End[a]

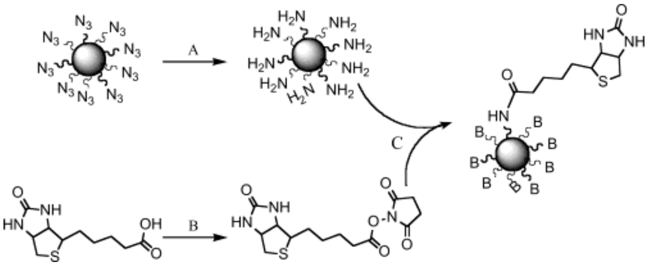

[a] Conditions: (A) THF, H_3PO_4 (0.65 M), PPh_3, 24 h; (B) biotin, TSTU, DIPEA, DMF, 4 h; (C) DMF, 24 h. (Note: B denotes biotin)

To confirm conjugation with biotin, residual amine groups on the particles were tagged with a fluorescent dye. Samples of the particles before and after the coupling step were treated with 5-fluorescein isothiocyanate (FITC) (Figure 2A). FITC is an organic dye commonly utilized in biological assays due to its efficient reactivity with primary amine groups and its large extinction coefficient, which allows it to be detected easily in low concentrations. Figure 2B shows the fluorescence spectra of the two types of nanoparticles displayed on the same scale. The intensity of the fluorescence maximum for the biotin-conjugated nanoparticles was appreciably less than that for the unconjugated nanoparticles, consistent with the conclusion that the majority of the amine groups were conjugated with biotin and therefore unavailable for reaction with FITC.

Silica surfaces are generally accepted to contain approximately five hydroxyl groups per nm^2.[41] The steric sizes of the PEG-**3** and PEG-**5** are significantly larger than a hydroxyl group, so the maximum theoretical coverage of PEG chains should be substantially less than five per square nanometer. A theoretical coverage was estimated by calculating the average hydrodynamic radius of the PEG chains in solution and then determining the number of such chains that could fit around the surface of the particle. The radius of gyration (R_g) of the PEG chains was calculated using the equation, $\langle s^2 \rangle = C_\infty n l^2/6$, in which C_∞ is the characteristic chain length of the polymer, n is the average degree of polymerization (DP) of the polymer chain, and l is the length per repeat unit. If the surface polymer layer existed in the mushroom regime, then the maximum surface coverage expected would be the surface area of the particle divided by the cross-sectional area of the PEG; $CA = \pi(R_g)^2$. If the surface polymer layer existed

---

(39) Farmer, S. C.; Patten, T. E. *Chem. Mater.* **2001**, *13*, 3920.
(40) von Werne, T.; Patten, T. E. *J. Am. Chem. Soc.* **2001**, *123*, 7497.
(41) Iler, R. K. *The Chemistry of Silica: Solubility, Polymerization, Colloid and Surface Properties, and Biochemistry*; John Wiley and Sons: New York, 1979.

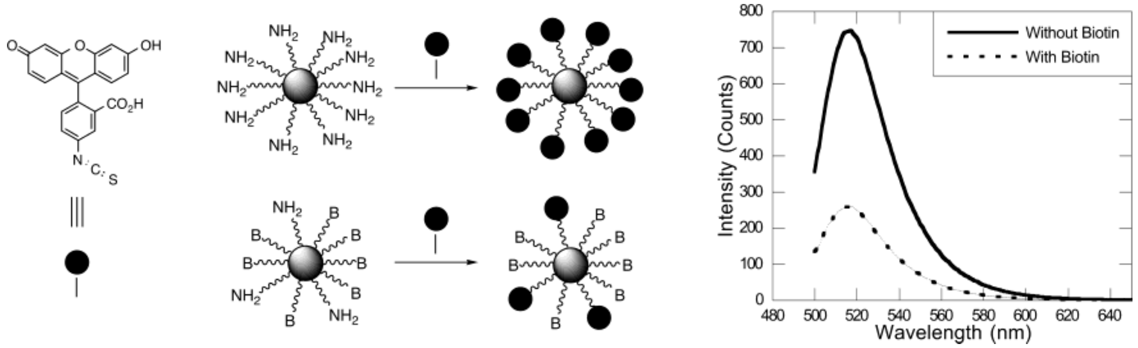

Figure 2. Schematic of reacting biotinylated and nonbiotinylated nanoparticle surfaces with fluorescein isothiocyanate (FITC). (Note: B denotes biotin.) On the right: Fluorescence emission spectra of FITC-tagged particles before biotinylation and after biotinylation.

Table 2. Biotin Surface Coverage of the PEG-Modified Nanoparticles

sample	NH_2 per particle[a]	biotin per particle		% conversion of amine end groups to biotin end groups[a]	area on surface per biotin (nm^2)
		theor[b]	expl[a]		
1	3100	4200	3000	~100	1.68
2	2000	2700	2100	~100	2.39
3	940	1300	500	53	10.05
4	200	380	100	50	50.27
5	0	0	0	N/A	0.00

[a] Based on FITC fluorescence experiments, elemental analysis, and IR spectroscopy. [b] Based on maximum loading of PEG linkers per particle (see the text).

in the brush regime, then the maximum surface coverage would be higher than this value. Calculations for the simplest case, sample 1 in Table 1, show that the theoretical maximum surface coverage for PEG-**3** in the mushroom regime would be 4200 per particle. The experimental surface coverage was determined to be 3000, which is a 71% surface coverage. Similar results were obtained from experiments in which mixtures of PEG-**3** and PEG-**5** were used to functionalize the particle surfaces. The theoretical functionality per particle was calculated using the equation $F_{\mathrm{part}} = (\mathrm{SA}_{\mathrm{part}}/\mathrm{CA}) \times$ %PEG-**3**, in which $\mathrm{SA}_{\mathrm{part}}$ is the surface area of the particle and %PEG-**3** is the relative amount of PEG-**3** with respect to the PEG-**5**. When combinations of PEG-**3** and PEG-**5** were used, the difference in chain lengths was taken into account by utilizing the weighted average of the two cross-sectional areas of the polymer chains, $\mathrm{CA} = (\%\mathrm{PEG}\text{-}\mathbf{3})(\mathrm{CA}_{\mathrm{PEG-3}}) + (\%\mathrm{PEG}\text{-}\mathbf{5})(\mathrm{CA}_{\mathrm{PEG-5}})$. Also, it was assumed that there was no difference in the kinetics of surface adsorption between the two PEG chains, so that the feed ratio of the two PEGs was the same as their incorporation ratio on the surface. Comparing the experimental and theoretical data in Table 2 showed that the efficiency of conjugation of the particle surface with biotin decreased with a decreasing amount of PEG-**3** on the surface. The reason for this behavior has not been determined, and the trend might be completely a result of the experimental error in measuring such a small amount of a functional group on the surface.

Once the biotinylated, water-soluble CdS@SiO_2 nanoparticles were synthesized, suspensions of nanoparticles were prepared and various concentrations of avidin were introduced. Because it has four biotin binding sites, avidin can act as a cross-linking agent and initiate the formation of nanoparticle aggregates. The property changing with time in these experiments is the overall size of the aggregates, so the experiments were monitored using dynamic light scattering (DLS). In all experiments, the number of particles present in solution and the total volume of solution were kept constant to allow for fair comparison between experiments utilizing particles of different extents of biotin functionality or differing avidin concentrations.

As a control experiment, the angular dependence of the intensity of light scattering, Γ, for the 40 nm CdS@SiO_2–PEG–biotin nanoparticles was measured. As shown in Figure 3a, the data could be fit with a linear function that, within experimental error, had a zero intercept, confirming that the individual particles behaved as spherical particles. Next, avidin was added to suspensions of the particles to initiate aggregation, and correlation functions were measured at 90° at various times. A composite plot is shown in Figure 3b that demonstrates that each curve was a single exponential function and that the functions broaden with time. These results are consistent with an increase in the average aggregate size over time and a relatively regular distribution of aggregate shapes.

Attempts to determine the angular dependence of the light scattering intensity for aggregates at different time intervals, and therefore different sizes, was not possible, because the time scale of such measurements was longer than the kinetic experiments. During the time needed to take the measurements at several angles, a significant change in the aggregate diameter occurred, thereby precluding any useful analysis of the data. Another complicating factor was that at sufficiently large sizes the aggregates began to precipitate from solution. This fact was observed by a notable appearance of cloudiness of the solution as well as in the behavior of the DLS data collected on the solution. Figure 4 shows a single experiment in which data were collected at multiple angles at various times. After 180 min the measured correlation functions were substantially broader than the baseline measurements, but after 6 h the measured correlation functions became more narrow and closer to the baseline measurements than the ones at 180 min. Such an observation might suggest that the size of the aggregates decreased over this time period, but this hypothesis was disproved by agitating the solution and reacquiring the data. The new correlation function was even broader than the one determined at 180 min. Therefore, the conclusion most consistent with the

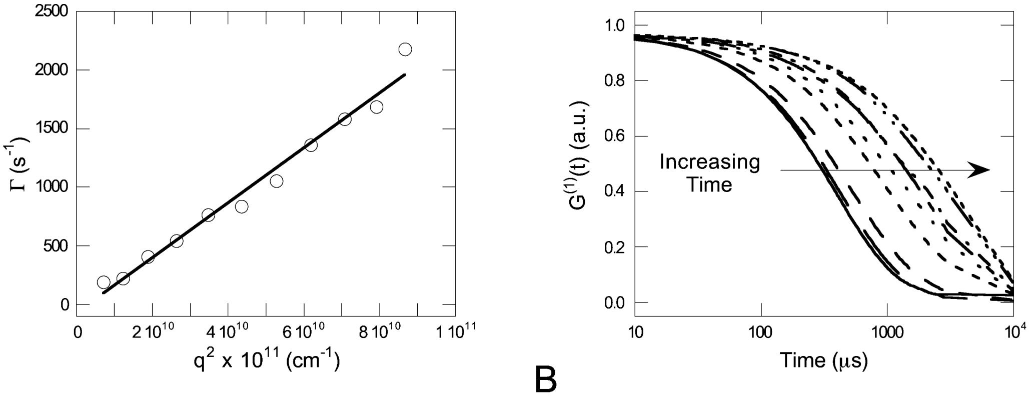

Figure 3. (A) Angular dependence of Γ for PEG-modified 40 nm CdS@SiO$_2$ nanoparticles. (B) DLS correlation functions as a function of time (measured at 90°) for sample 1 dispersed in a 170 nM avidin solution.

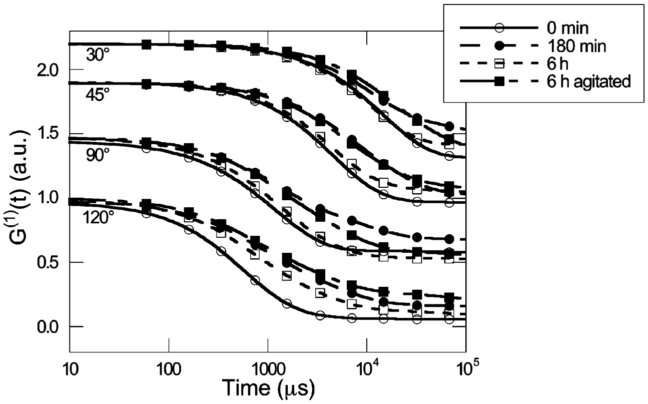

Figure 4. Correlation functions as a function of time and angle, showing the effects of large aggregate precipitation from solution and their resuspension upon agitation of the solution. Conditions: Sample 1 dispersed in a 170 nM avidin solution. (Note: measurements taken at 30°, 45°, and 90° were offset by 1.2, 0.9, and 0.5 au, respectively, for clarity.)

observations was that the aggregates at the higher end of the size distribution precipitated from solution over time and skewed longer time measurements to smaller diameter aggregates. TEM images of the supernatant and precipitate from one of these experiments further supported this conclusion (Figure 5). The image of the material that remained suspended in the supernatant revealed sub-micrometer-sized, fractal aggregates, whereas images of the material that precipitated out of solution showed aggregates that were significantly larger than a micrometer in diameter.

A procedure was developed in order to facilitate determining the angular dependence of the intensity of light scattering for the aggregates at different times. First, to avoid complications due to large aggregate precipitation, the collection of kinetic data was limited to short times (approximately less than 100 min). Second, the aggregation process was quenched at desired times by adding a 1000-fold excess of biotin to the reaction solution. The biotin present in excess occupied all remaining avidin sites and prevented the biotin groups on the particles from further reacting with the avidin. Figure 6A shows the correlation functions for four separate experiments that were quenched at four separate times. The effects of aggregate precipitation were observed only at times of 100 min or longer, so at shorter times data could be acquired successfully at multiple angles.

Figure 6B shows data for the angular dependence of Γ for a similar series of experiment using times shorter than 100 min, as well as linear fits of the data. The fact that the data could be fit using linear functions that have zero intercepts within experimental error demonstrated the success of the biotin quenching process, so diffusion coefficients and apparent hydrodynamic diameters of the aggregates can be calculated. More importantly, the data indicated that monitoring the aggregation kinetics using DLS at one angle (i.e., 90 °C) and then determining the slope of a line between that data point and the zero intercept should yield a reasonably accurate apparent hydrodynamic diameter with considerably less effort. As further demonstration of this point, Figure 6c shows the overlay plot of apparent hydrodynamic diameter versus time using data from the aggregation experiment performed in Figure 6b and a single experiment performed using similar concentrations of reagents, without biotin quenching, and while taking DLS measurements at 90°. The two experiments yielded the same slope within experimental error.

A series of aggregation experiments were performed in which the extent of biotin functionalization of the nanoparticle surface and the concentrations of avidin were varied. The particle concentrations were kept constant from experiment to experiment. Figure 7 shows the plots of apparent hydrodynamic diameter versus time obtained from the DLS measurements; the linear fits were added only to help identify the different sets of data and do not imply anything about the kinetic order of the process. A first inspection of the data showed that aggregation was observed for certain concentrations of avidin but not others. Further analysis showed that the rate of aggregate formation and the ultimate aggregate diameter were dependent upon the amount of biotin surface functionality as well as the avidin concentration. In separate experiments, aggregation was not observed either when avidin was not added to the nanoparticle sample or when avidin was added to the nanoparticle sample that did not contain any biotin surface functionality. Both of these control experiments indicated the necessary presence of the complimentary biotin-functionalized nanoparticle−avidin pair in order to observe aggregation.

Previous work on studying aggregates of nanoparticles utilized SEM and TEM to reveal the aggregate structure. In instances of fast, exponential aggregate growth, the observed structures were expanded and of

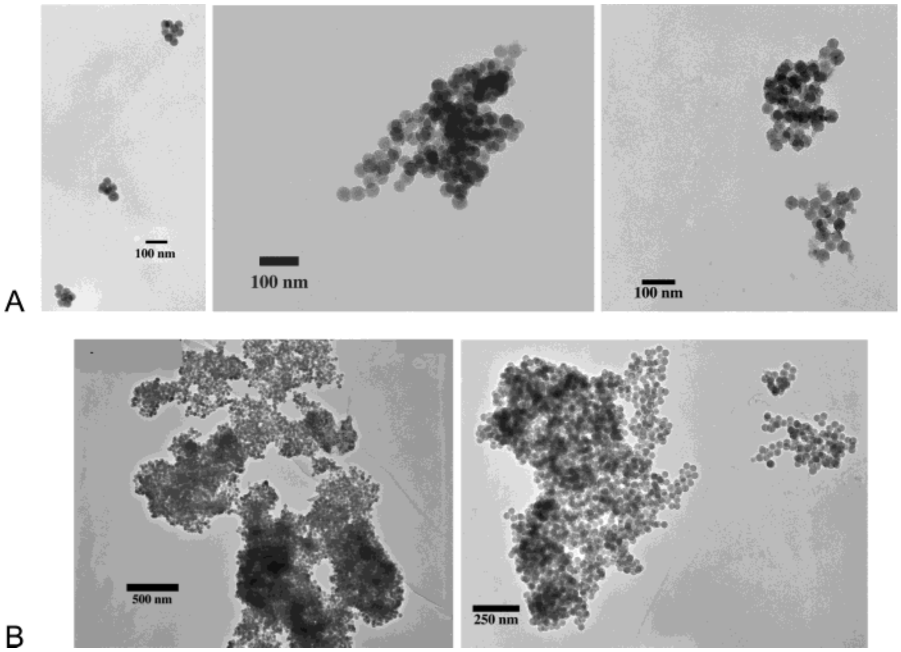

Figure 5. TEM analysis of the nanoaggregates isolated from the (A) supernatant and (B) precipitate of the experiment in Figure 5. Conditions: Sample 1 freeze-dried after 6 h from a 170 nM avidin solution.

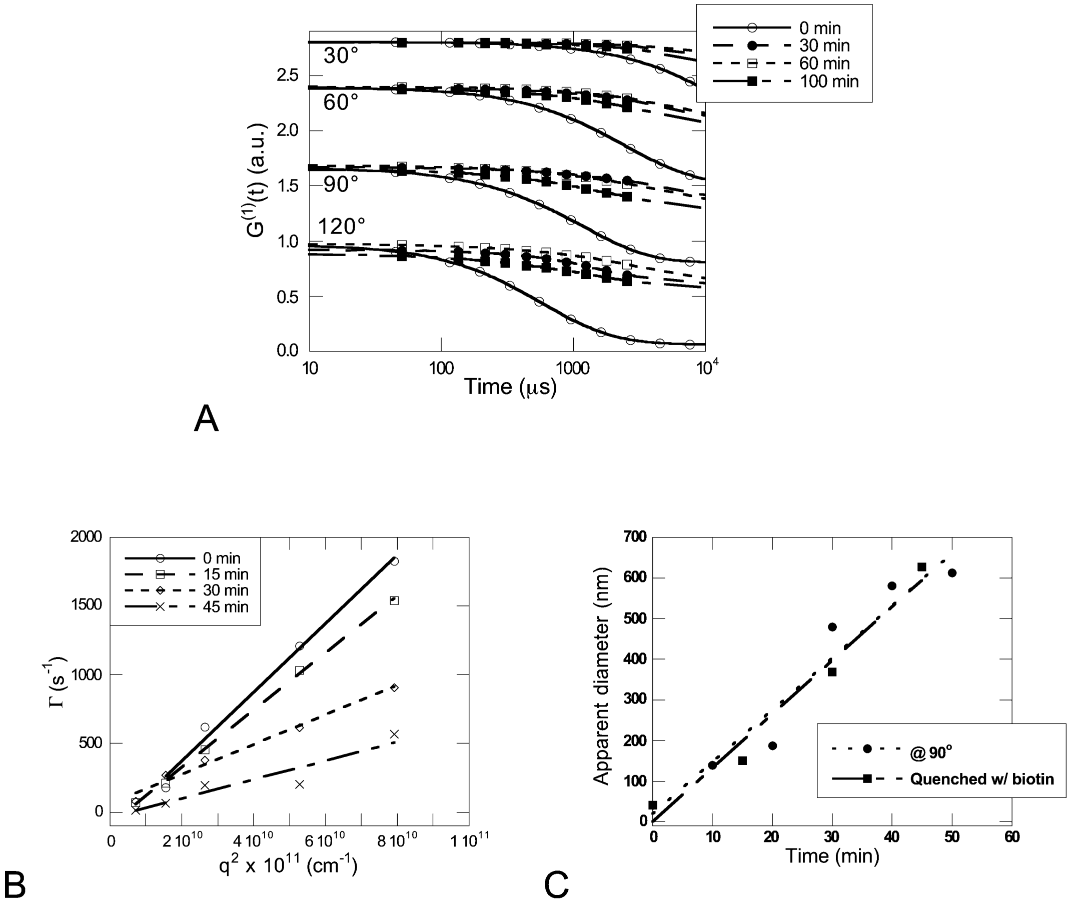

Figure 6. (A) Correlation functions as a function of time and angle for an aggregation experiment that was quenched with biotin at several times. Conditions: Sample 1 dispersed in a 170 nM avidin solution. (Note: measurements taken at 30°, 60°, and 90° were offset by 1.8, 1.4, and 0.7 au, respectively, for clarity.) (B) Angular dependence of Γ for aggregates that were quenched with biotin. Conditions: Sample 1 dispersed in a 170 nM avidin solution quenched with 0.3 mL of 0.175 mg/mL of biotin (1000-fold excess biotin). (C) Plots of apparent diameter versus time in which one set of data was recorded using measurements at 90° and the other set of data was recorded using multiple angle measurements.

lower fractal dimensions. Conversely, situations in which the rate of aggregate formation was slow, the observed structures were dense and of higher fractal dimensions.[42] SEM (Figure 8) and TEM (Figure 9) images of a representative sample of the aggregates formed during the experiments in Figure 7 revealed

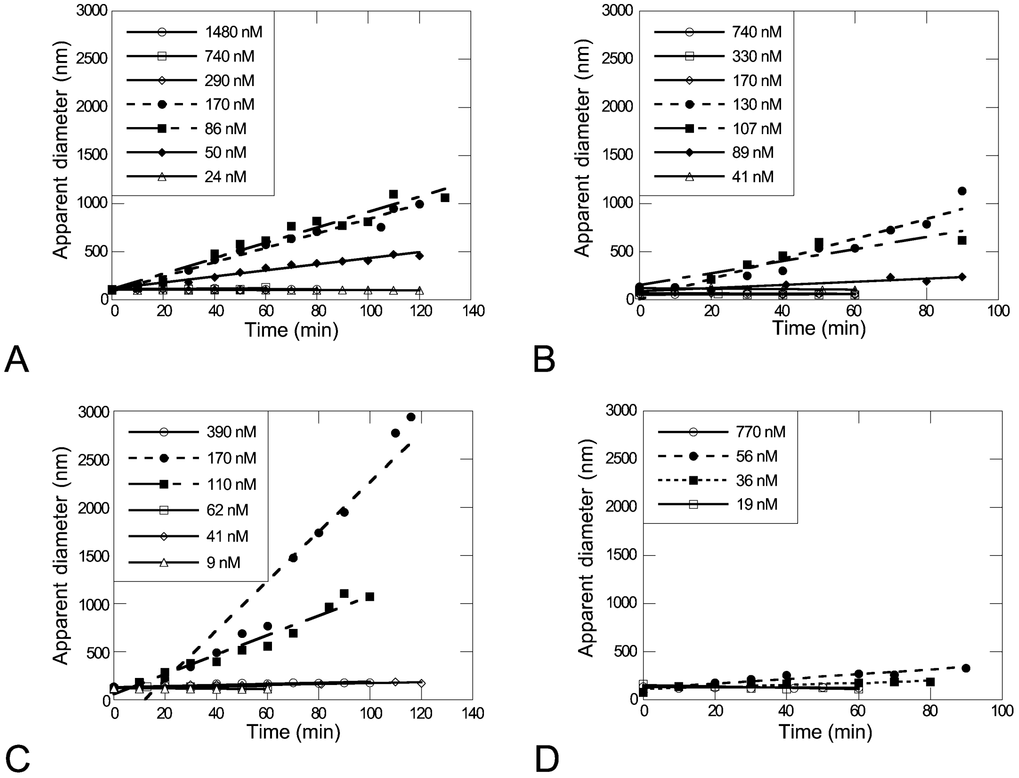

Figure 7. DLS analysis of aggregation experiments performed at various avidin concentrations. (A) Sample 1 (3000 biotin/particle); (B) Sample 2 (2100 biotin/particle); (C) Sample 3 (500 biotin/particle); (D) Sample 4 (100 biotin/particle). Conditions: 3 mL of 0.25 mg/mL of the respective sample, 1 mL of H_2O, and 1 mL of various avidin concentrations at room temperature.

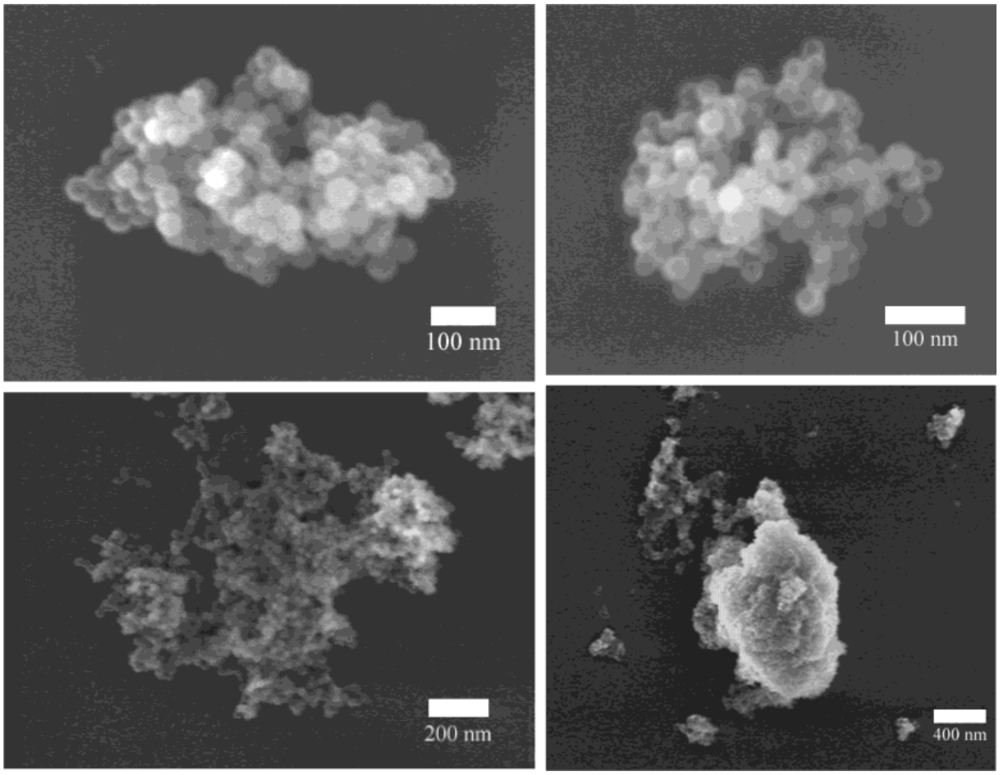

Figure 8. SEM analysis of nanoaggregates obtained using sample 1 freeze-dried after 2 h from a 87 nM avidin solution.

denser types of structures more consistent with a slow growth process and an appreciable distribution of aggregate sizes. TEM images of the control experiments only showed individual nanoparticles.

For simpler analysis of the kinetic growth data, the initial rates of aggregation (i.e., the slopes of the lines in Figure 7) were plotted against the avidin-to-particle

---

(42) Weitz, D. A.; Huang, J. S.; Lin, M. Y.; Sung, J. *Phys. Rev. Lett.* **1985**, *54*, 1416.

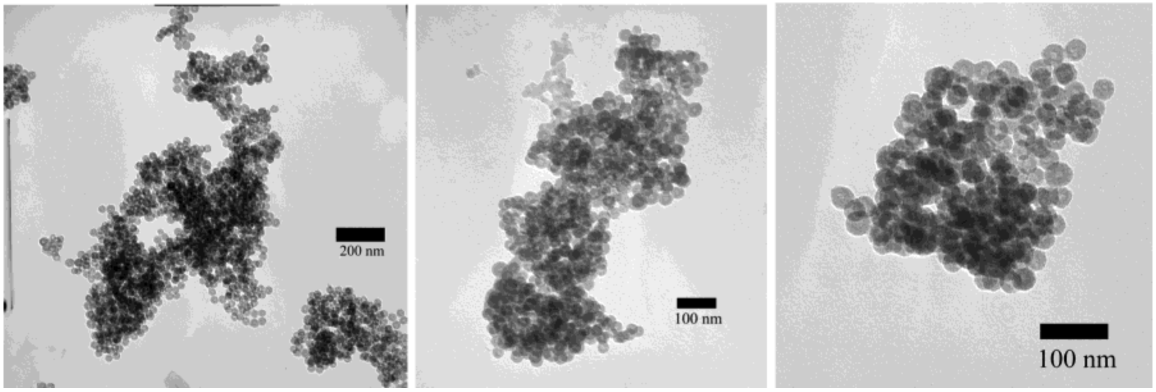

Figure 9. TEM analysis of nanoaggregates obtained using sample 1 freeze-dried after 2 h from a 87 nM avidin solution.

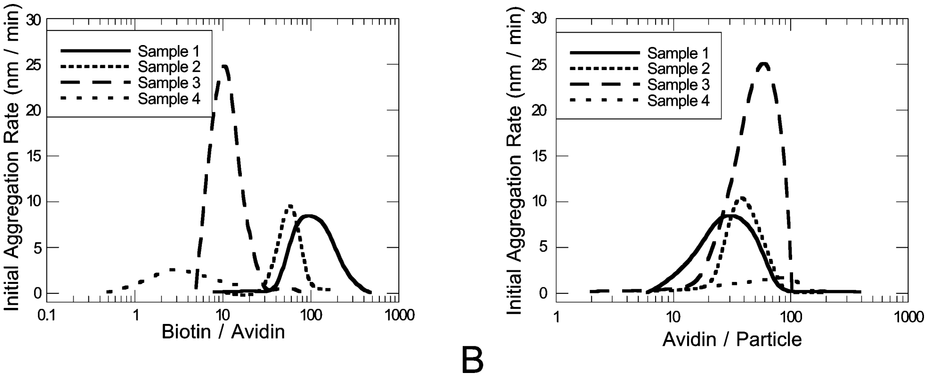

Figure 10. Dependence of the initial aggregation rate upon the (A) avidin-to-particle and (B) biotin-to-avidin ratios.

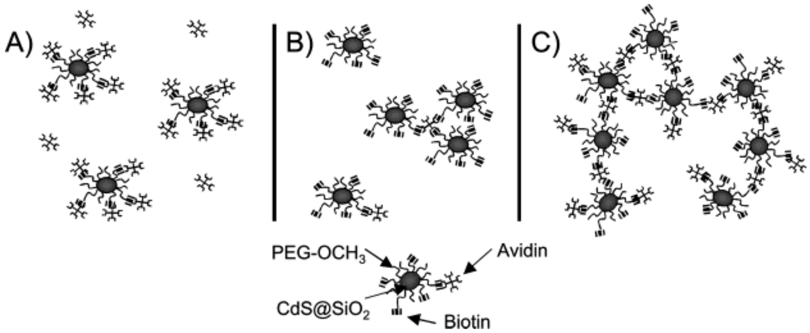

Figure 11. Schematic representation of functional group balance/imbalance when: (A) below the aggregation range, (B) above the aggregation range, and (C) within the aggregation range.

and biotin-to-avidin ratios (Figure 10). Only the first 60 min of each set of data was fit using a linear function, in order to preclude any possibility that precipitation would skew the results.

In each set of experiments a bell-curve distribution of initial aggregation rates was observed that was centered on an aggregation rate maximum (Figure 10). At low ratios of avidin per particle, no aggregation was observed, presumably because the initial concentration of avidin was very small and, therefore, very few interparticle cross-links could form (situation B in Figure 11). In this situation the particle surfaces contain either biotin with a small amount of avidin or just biotin. While the possibility of forming interparticle cross-links exists, there is too little avidin for many cross-links to form, and the rate at which biotin−avidin encounters occur is much too slow for aggregate growth. At very high initial concentrations of avidin, no aggregation was observed as well. Avidin is a much smaller object than the nanoparticle used in this experiment (~250 nm^3 versus 33 500 nm^3, correspondingly), and consequently, the protein can diffuse to the particle surface and bind much faster than the rate at which particles collide. Considering the large initial concentration of avidin, the particle surface rapidly becomes saturated under these conditions (situation A in Figure 11), such that the particle surface contains an excess of avidin binding sites over biotin groups. The number of possible cross-links is reduced which slows the aggregate growth. For initial concentrations of avidin between these two extremes, entitled “the aggregation range,” the fastest rate of aggregate growth was observed. After the avidin binds to the nanoparticle surfaces, there is a balance of avidin binding sites and biotin groups. Consequently, most particle collisions bring the complimentary groups together, a binding event occurs, and a cross-link is formed (situation C in Figure 11). The peak maximum of the curves shifted from low avidin-to-particle ratios for the particles with the highest biotin surface functionality to high avidin-

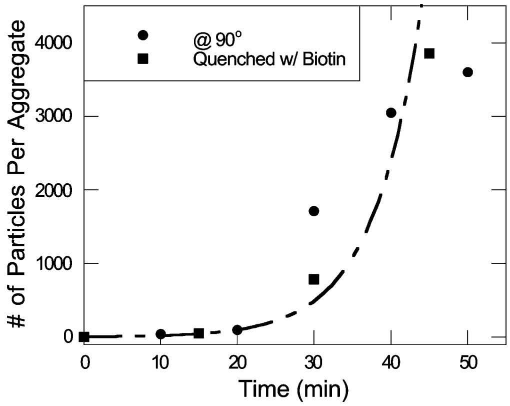

Figure 12. Replot of Figure 7c in which the *Y* axis was transformed into the number of particles per aggregate.

to-particle ratios for the particles with the lowest surface functionality, indicating that the system with the best sensitivity has the highest surface functionality.

When the data were plotted as initial aggregation rate versus the global biotin-to-avidin ratio (Figure 10B), the graph showed the cross-linking efficiency of each system more clearly. The peak maxima occurred at lower biotin-to-avidin ratios for particles with low surface biotin functionality and higher biotin-to-avidin ratios for the particles with the highest surface biotin functionality. The most efficient cross-linking occurred with the particles that had the lowest surface biotin functionality, because the global biotin-to-avidin ratio was closest to 4, the number of binding sites found in avidin. For the particles with the highest surface biotin content, the maximum aggregation rate occurred at a biotin-to-avidin ratio of 100-to-1. The reasons for such a disparity are probably numerous. First, when two particles bind together via an avidin cross-link, a certain area of biotin functional groups around the cross-linking site would be sterically blocked from binding more avidin. Second, previous studies on the chain dynamics of biotin end-functionalized PEGs binding to avidin functionalized micelles demonstrated that the PEG chain end can sample a range of distances away from the micelle surface.[43] Therefore, two biotin chain ends on the same particle surface could bind to the same avidin molecule and form a bridge structure rather than a cross-link. And finally, such bridge structures could also form over several other PEG chain ends and sterically prohibit those biotin groups from binding to an avidin. Each of these situations would occur frequently for particles with a high degree of biotin surface functionality and infrequently for particles with sparse biotin surface functionality, resulting in the latter system exhibiting the most efficient cross-linking.

The data in Figure 6c were replotted as the number of particles per aggregate per time (Figure 12), and the resulting graph showed that the number-averaged particle size increased as a power or exponential function with time. The rapid increase in particle size with time, the large size distribution of the final particles as observed in the TEM and SEM images, and the dense, fractal shape of the aggregates are all suggestive of a growth mechanism analogous to a step-growth polymerization in which there is one fundamental mechanistic step. Here, the step is the binding of biotin to avidin, and the dissociation constant for biotin−avidin is small, so one can consider this binding to be irreversible, particularly if two particles cross-link via multiple avidin molecules. So the growth mechanism for the system studied here is most likely a kinetically controlled process: instead of particles binding, dissociating, and rebinding such that thermodynamically favored packing is achieved, the particles colloid and bind in an essentially irreversible process. In contrast to the former situation, in the latter situation there is no possibility of having particle nucleation and growth separated in time or for an Ostwald ripening growth process, both of which would lead to a more uniform size distribution of roughly spherically shaped aggregates. As shown in Figure 13, we hypothesize that the growth mechanism in these studies involves individual particles colliding to form dimers and trimers and then progressively larger sized aggregates colliding and forming larger structures throughout the growth process. The larger structures would be agglomerates of smaller aggregates and would exhibit an irregular shape. At a certain point during the growth process, the largest particles in the size distribution become too large to remain suspended in solution, so they precipitate.

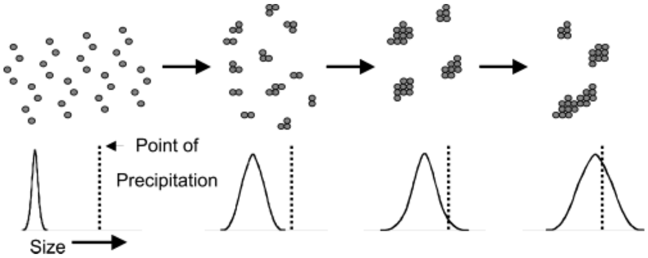

Figure 13. Schematic representation of the proposed kinetic growth mechanism for the formation of nanoaggregates (top) and of the change in size distribution of the aggregates with time (bottom).

Conclusions

Two difunctional, asymmetric PEG linkers were synthesized and utilized to prepare water-soluble, biotinylated CdS@SiO_2 particles with various surface contents of the biotin groups. Aqueous dispersions of these particles were prepared, and upon addition of avidin, aggregation was observed using DLS, TEM, and SEM analysis. The resulting aggregates were dense but also had fractal shapes. It was shown that single-angle DLS measurements at 90° were sufficiently accurate for quickly measuring the size of the aggregates as it evolved with time. Initial aggregation rates were measured as a function of surface biotin content of the nanoparticles and initial avidin concentration. The initial rates displayed bell-shaped curve responses to variations in the avidin-to-particle ratio and biotin-to-avidin ratio, the shapes of which were attributed to the stoichiometric balance/imbalance of the avidin-to-biotin ratio in the system and to intraparticle and interparticle bridges that could sterically block avidin from reaching some biotin sites. The growth mechanism was postulated to be a step-growth process.

---

(43) Jeppesen, C.; Wong, J. Y.; Kuhl, T. L.; Israelachvili, J. N.; Mullah, N.; Zalipsky, S.; Marques, C. M. *Science* **2001**, *293*, 465.

Experimental Section

Materials. All materials were purchased from commercially available sources and used without further purification. CdS@SiO$_2$ nanoparticles were prepared using a previously reported method.[39] Biotin-*N*-hydroxysuccinimide ester was synthesized using a known procedure.[44] Karstedt's solution was prepared as reported by Hitchcock and Lappert.[45]

Instrumentation. ^{1}H and ^{13}C {^{1}H} NMR spectra were recorded on a 300 MHz Varian instrument in CDCl$_3$. Chemical shifts, δ (ppm), were referenced to the residual solvent signal. IR samples were prepared neat on a salt plate, and analysis was conducted using an Matteson IR Galaxy Series FTIR 3000. Fluorescence measurements were conducted on a Perkin-Elmer LS50B using an λ_{ex} of 490 nm, 5 nm slit widths, and a step speed of 200 nm/min. Elemental analysis was conducted by Midwest Microlabs. Dynamic light scattering (DLS) analysis was conducted using a Brookhart Coherent DPSS 532 laser with a IEM 9863 detector (UC Davis) and a BI-200SM goniometer (Brookhaven Instruments) using a 2.5 W Ar laser light source (Model Innova 70-3 from Coherent) operating at 514.5 nm and a BI-9000 AT digital correlator (Brookhaven Instruments) (U Conn). Transmission electron microscopy (TEM) was conducted using a Phillips CM-12 TEM (UC Davis) and a Phillips EM 300 TEM (U Conn). Scanning electron microscopy (SEM) was conducted using an FEI XL30-SFEG. All microscopy samples were prepared by dipping carbon-coated copper grids into the appropriate solutions and then removing the water by freeze-drying.

Synthesis of α-Hydroxy-*ω*-azidopoly(ethylene glycol) (PEG-1). Poly(ethylene glycol) methacrylate (M_n = 360 g/mol; PDI < 1.05) (20.0 g, 55.6 mmol), *n*-propylamine (6.89 mL, 83.3 mmol), CH$_3$OH (100 mL), and a stir bar were placed into a 250 mL round-bottom flask, and the reaction mixture was stirred for 12 h. CH$_3$OH and excess *n*-propylamine were removed via rotary evaporation. THF (100 mL) and Et$_3$N (19.4 mL, 138.5 mmol) were added to the flask, which was cooled to 0 °C. Methanesulfonyl chloride (9.4 mL, 122.3 mmol) was added dropwise slowly. The flask was warmed to room temperature and stirred for 4 h. THF was removed via rotary evaporation and H$_2$O (70 mL) was added. NaHCO$_3$ was then added until a pH ~8 was reached. [**WARNING**: If azide is added to acid solutions, toxic and explosive HN$_3$ will form.] NaN$_3$ (4.30 g, 66.7 mmol) was added, and the reaction mixture was heated at ~90 °C for 8 h. The reaction was cooled to room temperature, K$_2$CO$_3$ (1.40 mM, 40 mL) was added, and then the solution was heated at ~100 °C for 12 h. The reaction was cooled to room temperature and extracted with CH$_2$Cl$_2$ (8×, 50 mL). The extracts were collected and dried over anhydrous MgSO$_4$. Solvent was removed to yield PEG-**1** (15.4 g, 88%). ^{1}H NMR: δ (ppm) 3.46 (36 H, br), 3.20 (2H, t). ^{13}C {^{1}H} NMR: δ (ppm) 72.7, 70.7, 70.4, 70.2, 61.6, 50.8. IR: ν (cm^{-1}) 3455 (br), 2900 (br), 2107 (sharp).

Synthesis of α-Allyl Ether-*ω*-azidopoly(ethylene glycol) (PEG-2). NaH (1.30 g, 32.4 mmol) and a stir bar were placed into a 50 mL round-bottom flask, which was vacuum/back-filled with N$_2$ (3×). PEG-**1** (3.40 g, 10.8 mmol) was dissolved in THF (25 mL), slowly added to the NaH, and stirred for 1 h at room temperature. Allyl bromide (2.80 mL, 32.4 mmol) was added slowly and the mixture stirred for 5 h. H$_2$O (50 mL) was then added very slowly to neutralize excess NaH. The reaction mixture was extracted with ethyl acetate (3×, 50 mL) and dried over anhydrous MgSO$_4$. Solvent was removed and the remaining product was freeze-dried from benzene to yield PEG-**2** (3.20 g, 88%). ^{1}H NMR: δ (ppm) 5.79 (1H, m), 5.11 (2H, dd), 3.91 (2H, d), 3.46 (22 H, br), 3.20 (2H, t). ^{13}C {^{1}H} NMR: δ (ppm) 134.9, 117.1, 72.4, 70.9, 70.7, 70.4, 70.2, 69.6, 68.2, 50.8, 25.9. IR: ν (cm^{-1}) 2900 (br), 2107 (sharp), 1645 (medium).

Synthesis of α-Dimethylethoxysilyl-*ω*-azidopoly(ethylene glycol) (PEG-3). PEG-**2** (6.30 g, 17.6 mmol), THF (1 mL), Karstedt's catalyst (88 μL), and a stir bar were placed into a 50 mL round-bottom flask. Dimethylethoxysilane (3.12 g, 83.0 mmol) was added slowly, and the reaction was heated to 80 °C for 18 h. Solvent was then removed via rotary evaporation, and the remaining product was freeze-dried from benzene to yield PEG-**3** (8.15 g, 97%). ^{1}H NMR: δ (ppm) 3.46 (22 H, br), 3.20 (2H, t), 1.15 (3H, t), 0.95 (2H, m), 0.48 (2H, m), 0.08 (6H, s). ^{13}C {^{1}H} NMR: δ (ppm) 74.2, 72.4, 70.9, 70.7, 70.4, 70.2, 69.6, 50.8, 31.2, 23.6, 18.9, 12.6, −1.8. IR: ν (cm^{-1}) 2900 (br), 2107 (sharp).

Synthesis of α-Allyl Ether-*ω*-methoxypoly(ethylene glycol) (PEG-4). Synthesis of PEG-**4** was similar to that of PEG-**2**, using poly(ethylene glycol) methyl ether (M_n = 350 g/mol, PDI < 1.05) (5.00 g, 14.3 mmol) to yield PEG-**4** (4.9 g, 88%). ^{1}H NMR: δ (ppm) 5.51 (1H, m), 5.11 (2H, dd), 3.87 (2H, d), 3.46 (20 H, br), 3.11 (3H, s). ^{13}C {^{1}H} NMR: δ (ppm) 134.9, 117.1, 72.4, 70.9, 70.7, 70.4, 70.2, 69.6, 25.9. IR: ν (cm^{-1}) 2900 (br), 1620 (medium).

Synthesis of α-Dimethylethoxysilyl-*ω*-methoxypoly(ethylene glycol) (PEG-5). Synthesis of PEG-**5** was similar to that of PEG-**3**, using PEG-**4** (4.9 g, 12.6 mmol) to yield PEG-**5** (5.56 g, 90%). ^{1}H NMR: δ (ppm) 3.46 (20 H, br), 3.20 (2H, q), 3.18 (3H, s), 1.15 (3H, t), 0.95 (2H, m), 0.48 (2H, m), 0.08 (6H, s). ^{13}C {^{1}H} NMR: δ (ppm) 72.4, 70.9, 70.7, 70.4, 70.2, 69.6, 58.4, 31.2, 23.6, 18.9, 12.6, −1.8. IR: ν (cm^{-1}) 2900 (br).

Preparation of CdS@SiO$_2$−PEG−N$_3$. CdS@SiO$_2$ nanoparticles, THF (100 mL), difunctional PEG linkers, and a stir bar were loaded into a 250 mL round-bottom flask and refluxed for 72 h. Excess solvent was removed by rotary evaporation, and the particles were isolated by a series of centrifuge/decant/resuspend cycles (5×) with CH$_3$OH/hexane/THF (1:1:3). Particles were dried under vacuum and analyzed by elemental analysis (See Table 1) and IR spectroscopy (presence of N$_3$ stretch at ~2110 cm^{-1}).

Preparation of CdS@SiO$_2$−PEG−NH$_2$. CdS@SiO$_2$−PEG−NH$_2$, THF (45 mL), and a stir bar were loaded into a 100 mL round-bottom flask. PPh$_3$ (0.52 g, 2 mmol) was added to the flask, followed by H$_3$PO$_4$ (0.65 M, 25 mL), and the mixture was stirred for 24 h. Particles were isolated by a series of centrifuge/decant/resuspend cycles (5×) with CH$_3$OH/hexane/THF (1:1:3). Particles were dried under vacuum and analyzed by elemental analysis (See Table 1) and IR spectroscopy (absence of N$_3$ stretch at ~2110 cm^{-1}).

Preparation of CdS@SiO$_2$−PEG−Biotin. Biotin-*N*-hydroxysuccinimide ester was generated and then transferred to a 100 mL round-bottom flask containing CdS@SiO$_2$−PEG−NH$_2$ suspended in DMF (45 mL), and the mixture stirred for 24 h. Particles were isolated by a series of centrifuge/decant/resuspend cycles (5×) with CH$_3$OH/hexane/THF (1:1:3) and dried under vacuum.

Determination of Biotin Functionality. Nanoparticles with amine functionality (50 mg) were suspended in DMF (5 mL) in a 10 mL round-bottom flask to which 5-fluorescein isothiocyanate (FITC) (10 mg) was added, and the reaction was stirred for 24 h. In a second 10 mL round-bottom flask, nanoparticles with biotin functionality (50 mg) were suspended in DMF (5 mL) in a 10 mL round-bottom flask to which FITC (10 mg) was added, and the reaction was stirred for 24 h. Particles were isolated by a series of centrifuge/decant/resuspend cycles (5×) with CH$_3$OH/hexane/THF (1:1:3) and dried under vacuum. Solutions of identical concentrations were then prepared and analyzed by fluorimetry.

Typical Aggregation Experiment. Test tubes were prepared by inversion of the tube upon a small glass stir rod. Rods were placed into a 500 mL beaker with approximately 50 mL of THF. The beaker was covered with a watch glass, and the solvent was heated at reflux for at least 10 min. Into the cleaned tubes, H$_2$O (1 mL) and a CdS@SiO$_2$ suspension (3 mL, 0.25 mg/mL) were passed through a 0.45 μm filter. An initial particle size was determined, which was followed by the addition of an avidin solution (1 mL) of various concentrations through a 0.45 μm filter into the cleaned test tube. In all experiments, the final volume size was 5 mL. The size of the

---

(44) Bannwarth, W.; Knorr, R. *Tetrahedron Lett.* **1991**, *32*, 1157.

(45) Hitchcock, P.; Lappert, M.; Warhurst, N. *Angew. Chem. Int. Ed. Engl.* **1991**, *30*, 438.

aggregates was monitored over time by dynamic light scattering measurements.

Typical Biotin Quenching Experiment. Test tubes were prepared as described above, as was the preparation of the aggregate solution. The reaction mixture was immediately divided into various aliquots of equal volumes. To these, 0.30 mL aliquots of 0.175 mg/mL biotin were added at various times. The size of the aggregates was determined by dynamic light scattering measurements.

Acknowledgment. We would like to thank Mike Dunlap and Chris Chervin for assistance acquiring the SEM images and Mark Jordi for help in acquiring the TEM images in Figure 5. We recognize Professor Rosemary Smith and Professor Scott Collins for helpful discussions. This work was supported by NSF (CAREER DMR-97-33786) and NEAT-IGERT (DGE−9972741).

CM049811I